DOI:
10.1002/jbio.201960099

Document Version
Peer reviewed version

Received September 2019; | Revised: 00 Month 0000 | Accepted: 00 Month 0000

DOI: xxx/xxxx

FULL ARTICLE

Lightsheet fluorescence lifetime imaging microscopy (FLIM) with wide-field time-correlated single photon counting (TCSPC)

Liisa M. Hirvonen*[1] | Jakub Nedbal[2] | Norah Almutairi[3] | Thomas A. Phillips[1] | Wolfgang Becker[4] | Thomas Conneely[5] | James Milnes[5] | Susan Cox[1] | Stephen Stürzenbaum[3] | Klaus Suhling**[2]

[1]Randall Centre for Cell and Molecular Biophysics, King's College London, Guy's Campus, London SE1 1UL, U.K.
[2]Department of Physics, King's College London, Strand, London WC2R 2LS, U.K.
[3]School of Population Health & Environmental Sciences, Faculty of Life Sciences & Medicine, King's College London, 150 Stamford Street, London SE1 9NH, U.K.
[4]Becker & Hickl GmbH, Nunsdorfer Ring 7-9, 12277 Berlin, Germany
[5]Photek Ltd., 26 Castleham Rd, Saint Leonards-on-Sea TN38 9NS, U.K.

Correspondence
**Corresponding author. Email: klaus.suhling@kcl.ac.uk

Present Address
*Centre for Microscopy, Characterisation and Analysis (CMCA), The University of Western Australia, 35 Stirling Highway, Perth WA 6009, Australia

We report on wide-field time-correlated single photon counting (TCSPC)-based fluorescence lifetime imaging microscopy (FLIM) with lightsheet illumination. A pulsed diode laser is used for excitation, and a crossed delay line anode image intensifier, effectively a single-photon sensitive camera, is used to record the position and arrival time of the photons with picosecond time resolution, combining low illumination intensity of microwatts with wide-field data collection. We pair this detector with the lightsheet illumination technique, and apply it to 3D FLIM imaging of dye gradients in human cancer cell spheroids, and *C. elegans*.

KEYWORDS:
Lightsheet microscopy, SPIM, fluorescence lifetime imaging (FLIM), time-correlated single photon counting (TCSPC), microchannel plate (MCP)

1 | INTRODUCTION

The observation of cells and organelles in their native 3D environment is becoming increasingly important in biological research.[1] Fluorescence microscopy provides a way to do this, as it is a minimally invasive, non-destructive and non-ionising tool which can be used to study living cells and tissues with negligible cytotoxicity, so that dynamics and function can be observed and quantified. No other method can study molecules in living cells with anything remotely approaching its combination of spatial resolution, selectivity, sensitivity and dynamics.

In a conventional fluorescence microscope, the sample is typically placed on a glass coverslip, and imaging is restricted to a region relatively close to the coverslip, as resolution and contrast decrease rapidly with imaging depth, which can be problematic for larger samples. Also bleaching and phototoxicity can become issues in 3D imaging due to prolonged illumination of the whole sample volume. Multiphoton excitation microscopy helps to address these issues, and can image relatively large samples when using a mesolens.[2,3] This is a scanning approach where the image is acquired pixel by pixel. To acquire the whole field of view in a single exposure using a camera while still addressing the photobleaching and depth issue, lightsheet illumination can be used.

In the past ten years, developments in lightsheet illumination techniques have advanced biological 3D microscopy enormously. Also called single/selective plane illumination microscopy (SPIM) and named Nature Methods "Method of the Year 2014",[4] lightsheet microscopy provides inherent optical sectioning and reduces photobleaching outside the focal plane. While the sideways illumination technique is not new – it was first introduced in 1902 by Zsigmondy to look at scattered light from colloids in solutions, for which he won the Chemistry Nobel prize in 1925[5] – its recent re-discovery and utilisation in fluorescence microscopy has become a powerful and popular technique. It allows image acquisition with depth resolution provided by the illumination lightsheet, without bleaching the parts of the sample that are not imaged. It is typically applied to biological imaging of larger multicellular organelles, such as cell clusters, tissues or embryos, with low magnification and a large field of view, but it also has applications in single cell imaging. Indeed, lightsheet microscopy has been demonstrated in single molecule scale and combined with superresolution microscopy.[6] It can be performed over long periods of time with very low phototoxicity. Typically, the sample is mounted in a highly viscous medium such as agarose gel, placed in a small transparent tube and mounted in front of the camera (see Fig 1 inset). It is possible to rotate the sample and acquire three-dimensional stacks from various angles. There are many different practical implementations of lightsheet microscopy, each with their benefits and drawbacks and suitability for a specific application.[7] As it is not based on point-scanning an excitation beam, it usually requires a camera to acquire the image.

Fluorescence lifetime imaging microscopy (FLIM) provides contrast according to the time the fluorophore spends in the excited state. This often depends on the microenvironment of the probe, such as oxygen or ion concentration, pH, viscosity, temperature, or proximity of other fluorophores. A great advantage of combining FLIM with lightsheet microscopy is that it enables functional imaging, i.e. it can go beyond the structural and morphological information that is obtained from standard implementations of lightsheet microscopy. There are some reports on combining lightsheet illumination with FLIM, usually either with frequency domain[8,9] or time-gated FLIM[10,11] approaches,[12–15] but only one report, to the best of our knowledge, on the use of time-correlated single photon counting (TCSPC) for lightsheet FLIM microscopy.[16] The authors use a prototype image intensifier with capacitive division imaging readout technique, which is based on charge division to determine the photon position and arrival timing.[17] They image fluorescent beads and a calcium sensitive dye in buffer solution of varying calcium ion concentrations, and drosophila larvae.

TCSPC has been reported to have the best signal-to-noise ratio of the standard time-resolved imaging methods. It is independent of excitation intensity variations, and its other key advantages stemming from its digital nature include single photon sensitivity, a high dynamic range, linearity, well-defined Poisson statistics and easy visualisation of photon arrival time data.[18,19] FLIM is often implemented in a scanning system, but there are also many methods to perform wide-field TCSPC.[20] Traditionally, microchannel plate (MCP) detectors have been used for timing photon arrival with precision of few tens of picoseconds.[21] To also record the position, different read-out anode architectures have been developed.[22–25] Quadrant anodes have been used for long-term wide-field TCSPC FLIM imaging with low excitation intensity.[26–28] In a delay line anode detector, the problem of determining the position of the photon is converted into a timing problem. We have previously shown that this type of detector can be read out with standard TCSPC timing electronics, e.g. timing boards that are routinely used for fluorescence decay measurements, for example in combination with scanning FLIM.[29] We have also employed this detector for total internal reflection FLIM, a method that typically requires a camera.[30]

The trend towards higher resolution and ever thinner optical sections and the limited photon budget available from fluorophores make photon counting the method of choice for lightsheet FLIM. In this work we have combined wide-field TCSPC FLIM with lightsheet illumination using two orthogonal objectives. For TCSPC detection, we have combined a microchannel plate (MCP)-based detector with a delay line position sensitive anode and fast electronics.[29,30] This detection system allows wide-field FLIM with picosecond time resolution and extremely low illumination intensity. We employ this detector on lightsheet illumination microscope, and apply this system to FLIM of human cancer cell spheroids and *C. elegans*.

2 | METHOD

2.1 | Microscope setup

The lightsheet microscope setup is based on the openSPIM[31] setup geometry, see Fig 1 . A Horiba DeltaDiode picosecond diode laser with 485 nm head (DD-485L) was used for excitation at 10 MHz repetition rate. A 475/28 filter was inserted in front of the laser, and neutral density filters were used in the excitation path to reduce the illumination intensity. The beam was expanded with two lenses (f_1=50 mm, f_2=100 mm), the lightsheet was created with a slit and a cylindrical lens (f_c=50 mm), and the beam

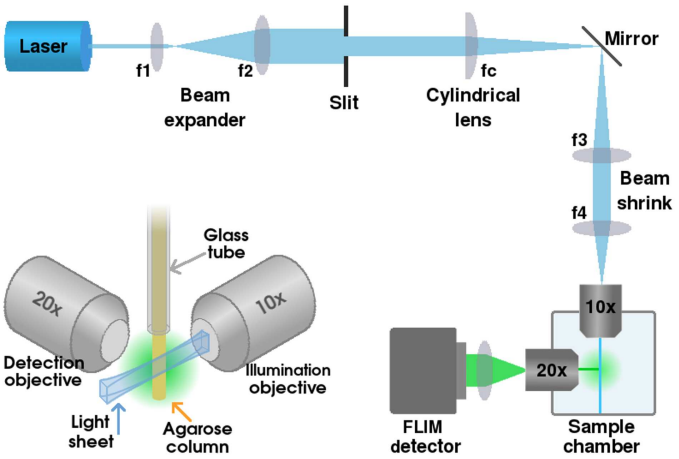

FIGURE 1 Schematic diagram of the lightsheet FLIM microscope setup. Inset: The sample is mounted in an agarose column and placed on the intersecting focal planes of the illumination and detection objectives.

diameter was then decreased with another two lenses (f_3=100 mm, f_4=50 mm). The lightsheet was focused onto the sample with a 10× NA0.3 water immersion objective (UMPLFLN10XW, Olympus), mounted onto the side of a water-filled sample chamber. The fluorescence from the sample was collected with a 20× NA0.5 water immersion objective (UMPLFLN20XW, Olympus), mounted onto another side the sample chamber perpendicular to the excitation objective such that their focal planes intersect. A 515 nm long-pass emission filter (FITC-LP01-Clin-25, Semrock) was placed in the emission path, and the image was focused onto the detector with a tube lens (TTL200-A, Thorlabs).

For imaging, the sample chamber was filled with deionised water (or M9 buffer for *C. elegans*). The samples were suspended in agarose (RC-122, G-Biosciences) and mounted into 1 mm diameter glass capillaries (701904, Brand). The capillaries were mounted on a micrometer stage on top of the sample chamber such that the end of the capillary was slightly above the focal plane of the objectives, and the agarose was then pushed out of the capillary into the beam path where the focal planes of the objectives intersect (see Fig 1 inset).

2.2 | FLIM detector

The delay line detector used in this work has been described in detail elsewhere.[29,30] Briefly, the 40 mm double MCP detector (Photek, UK) was combined with a 4-channel delay line read-out anode structure (DLD40, Roentdek, Germany) located outside the tube and coupled capacitively to a resistive anode inside the tube using image charge technique.[32,33] The output signal from the MCP before the anode (time channel) was input to a SPC-150 TCSPC module (Becker & Hickl, Germany), and the timing done in the conventional way.[18] The delay line output signals (X0, X1, Y0 and Y1) were connected to constant fraction discriminators (CFDs) and amplifiers (Roentdek, Germany) that were optimised for slow pulse rise times as detailed in[29] and then connected to two SPC-150 TCSPC modules (Becker & Hickl, Germany), one for X and one for Y.

X1 and Y1 signals were connected to the signal inputs, and the stop signals were obtained from X0 and Y0 after passing through a 10 meter delay cable. This ensures that the X1 and Y1 signals always arrive first and start the TCSPC boards' time-to-amplitude converters, and the X0 and Y0 signals stop them. This setup thus measures the propagation time difference of the signal along the delay line, and therefore the photon event location. Data was collected with SPCM instrument control software (Becker & Hickl, Germany).

2.3 | Data processing

Data was recorded in first-in first-out (FIFO, Parameter-Tag) mode, where each SPC-150 card writes a data file with two time stamps for each photon: microtime (time since the last excitation pulse) and macrotime (time since the start of the experiment). The three output files were combined by finding events that were found in the same macrotime window, corresponding to the time between laser pulses, in all three input files. The result file then only has photon events which were detected in all three (x, y and t) channels.[18] Due to the broad pulse height distribution of the MCP and ringing in the pulse shape caused by the delay

line structure, not all events are detected in all three channels. The 100 ns detection window was divided into 512 bins (pixels) for the x, y and t channels, thus yielding a calibration of 0.1953 ns/channel.

For the creation of the lifetime images, the photons were placed into an xyt data cube, and the data written into an .ics image file. The fluorescence decay in each pixel of the image was fitted with a monoexponential or biexponential function using Tri2[34] or SLIM Curve[35] software, and the lifetime encoded in a pseudocolor scale (blue for short lifetimes and red for long lifetimes). The lifetime and intensity images were combined by weighting the lifetime image pixel brightness values by the fluorescence intensity image. Average lifetimes for biexponential fits were obtained from the intensity-averaged fluorescence lifetime $\tilde{\tau} = \frac{\alpha_1\tau_1^2+\alpha_2\tau_2^2}{\alpha_1\tau_1+\alpha_2\tau_2}$.[36] For volume sweep imaging, lifetime τ was calculated using the method of moments.[37,38] The first moment of the photon distribution is defined as $M_1 = \frac{\sum N_i t_i}{N}$, where t_i is the time of the time channel i, N_i is the number of photons in time channel i, and N is the total number of time channels. τ was then obtained from the difference between the fluorescence decay and IRF: $\tau_{M1fluo} - \tau_{M1IRF}$.

2.4 | Sample preparation

2.4.1 | Beads

Two different types of fluorescent bead samples were used for testing the setup. For the first sample, two types of green fluorescent beads with 10 μm diameter (G1000, Thermo Fisher Scientific and 94050, Sigma-Aldrich) were mixed and suspended in agarose (A9414, Sigma Aldrich). For the second sample, fluorescent 1 μm beads (F8823, Invitrogen) and quantum dots (Lumidot CdSe/ZnS, 694649, Sigma) were mixed such that they spontaneously formed aggregates in the agarose.

2.4.2 | Cancer cell spheroids

MCF-7 cells (ATCC HTB-22) were cultured in 37°C, 5% CO_2 in EMEM supplemented with 10% FBS, 1% penicillin/streptomycin, and 1% L-glutamine. For MCF-7 cell line with stable GFP-lifeact expression, lentivirus encoding lifeact-GFP[39] (a gift from R. Wedlich-Soldner, Max Planck Institute of Biochemistry, Martinsried, Germany) was packaged in HEK293T cells by transient transfection, and the supernatants containing lentivirus harvested after 48 h. The MCF-7 cells were then incubated with lentiviral supernatants for 24 h, and sorted for optimal GFP expression. Spheroids were prepared by the hanging drop method adapted from[40]. For the methylcellulose (MC) stock 6 g was dissolved in 250 ml DMEM and stirred for 20 minutes at RT, the solution was then stirred overnight at 4°C with additional 250 ml of DMEM and clarified by centrifuging. 150,000 cells were suspended in 3 ml of 25% MC in growth medium, and 30 μl drops were deposited onto the lid of a square petri dish. The lid was then inverted over the dish bottom containing PBS, and the hanging drops incubated at 37°C, 5% CO_2 to allow spheroids to form. After 24 h the spheroids were fixed in 4% formaldehyde for 2 h and washed thoroughly. For spheroid surface labelling Alexa488-conjugated Tom20 antibody (sc-17764-AF488, Santa Cruz Biotechnology) was diluted 1:25 in PBS and the spheroids incubated for 1 h. The samples were washed thoroughly, mounted into agarose and imaged immediately.

2.4.3 | *C. elegans*

The standard method by Brenner[41] was used to culture a transgenic *Caenorhabditis elegans* strain which expresses *Pmtl*-1::GFP only upon exposure to cadmium. Synchronized (L1 stage) larva of the transgenic worms were grown on Nematode Growth Media (NGM) and fed ad libitum with *E. coli* OP50 in the presence or absence of 60 μM cadmium chloride (Sigma-Aldrich 99% A.C.S - $CdCl_2$). The nematodes were collected after 27 hours (L3 stage), then washed multiple times with M9 buffer at room temperature to remove residual *E. coli* OP50.[42] A subsection of nematodes (grown with or without cadmium supplementation) were suspended in 1 ml of M9 buffer containing 2 μl of acridine orange (0.03 g/2 ml) (Cambridge Bioscience) at room temperature (in the dark) for 1 hour. To remove excess amounts of the dye, worms were subsequently washed two times with M9 buffer and transferred to fresh NGM plates for 1 hour at 20°C. Next, the worms were collected and washed multiple times to remove *E. coli* OP50, then suspended in 1 ml of M9 buffer containing sodium azide (5mM NaN_3). Agarose (2%) was added to the immobilized worms at a ratio of 1:1 and the mixture loaded inside the glass capillary.

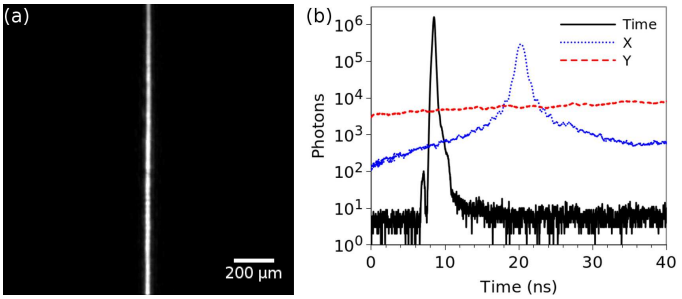

FIGURE 2 Characterisation of the microscope measured by placing a mirror in the sample holder at at an angle of 45°. (a) Image of the lightsheet. (b) Distribution of photons in the time (black), x (blue) and y (red) channels show the IRF in the time channel and cross-section of the lightsheet in the x channel. The actual measurement period is 100 ns; the edges have been left out for clarity.

3 | RESULTS

3.1 | Calibration

For the measurement of the lightsheet thickness and the instrument response function (IRF), a mirror was placed in the sample plane at at an angle of 45°, and the emission filter replaced with a strong neutral density filter. Data was acquired for ∼5 minutes, with 16.6 million matched photons and count rate of 56.2 kHz. The event acceptance rates for the individual channels were 88.9% for x, 86.0% for y, and 80.2% for the time channel. Fig 2 a shows an image of the reflected lightsheet, and Fig 2 b shows the photons collected in the time channel corresponding to the IRF (black line), in the x-channel corresponding to the cross-section of the lightsheet (blue line), and in y-channel which shows no features (as expected for a cross section of the image along the lightsheet). The IRF measured full width at half maximum (FWHM) is 288 ps, and the lightsheet thickness ∼21 μm.

3.2 | Fluorescent beads

3.2.1 | Slice-by-slice imaging

The lightsheet FLIM setup was first tested with a sample containing two types of green fluorescent beads which are difficult to distinguish by their emission spectrum. A stack was acquired with 10 μm spacing with a total of 44 slices and 2 minutes acquisition time per slice. Intensity and lifetime images of a slice from this stack are shown in Figs 3 a-c. The lifetime images were obtained by fitting a single exponential function to each pixel of the image. Example decays for areas indicated in Fig 3 b and monoexponential fits to these decays are shown in Fig 3 d, yielding average lifetimes of 2.21±0.04 and 3.54±0.14 ns for the two types of beads. The lifetime histogram of the whole stack (Fig 3 e) shows two peaks at 2.23 ns and 3.56 ns, as expected, corresponding to the lifetimes of the two different beads, and, as the density of the beads was quite high such that there is overlap between beads, a distribution of lifetimes between these two values corresponding to pixels that have a contribution from both lifetimes. See Supplementary Information for the full stack.

3.2.2 | Volume sweep imaging

The lightsheet FLIM microscope can be operated at volume sweep imaging mode, where the sample is moved at constant speed through the lightsheet and data is acquired at a constant stream, and later divided onto slices of required duration. This method was tested with a sample containing a mix of fluorescent beads and quantum dots. A total of 11.3 million photon events were detected in all three (time, x and y) channels during the 6 minutes data collection time, with count rate of 31.6 kHz. The photons were divided into frames of 330 ms, corresponding to a distance of 0.5 μm, with 900 frames in total. The lifetime in each pixel of this xyzt data stack was then calculated using the method of moments. Fig 3 f shows volume rendering of the intensity-weighted lifetime image stack, and Figs 3 g-i cross-sections of this stack in x, y and z dimensions. Although both species emit in green and are difficult to distinguish by colour or intensity, the lifetimes are different, and the image shows clear lifetime contrast between the beads that have a shorter lifetime and the quantum dots with a longer lifetime.

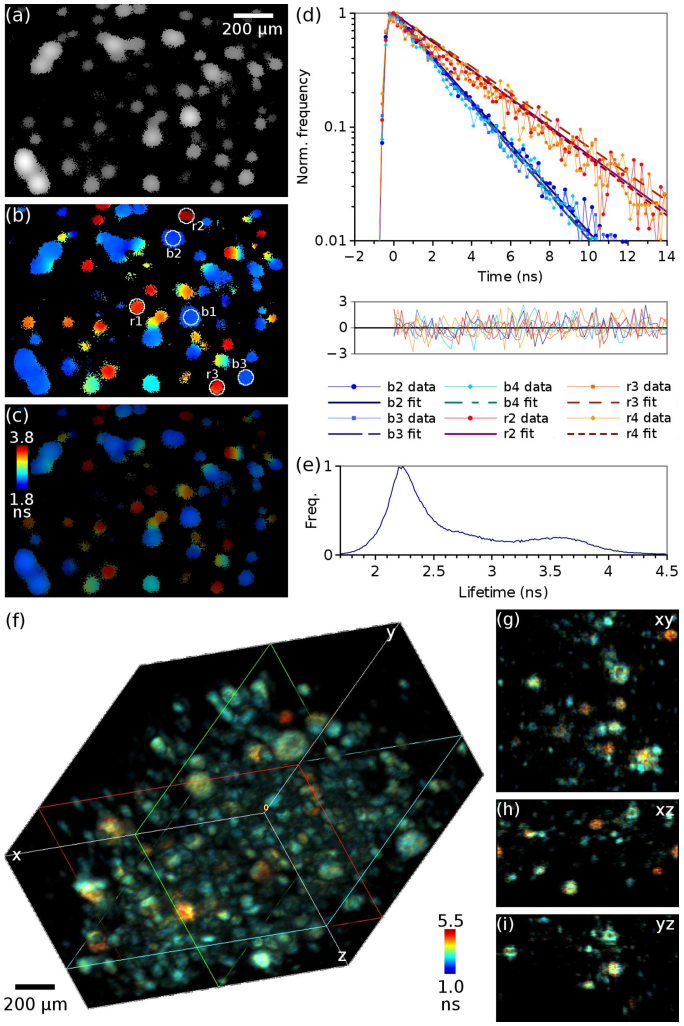

FIGURE 3 Fluorescent beads imaged with the lightsheet FLIM microscope. (a) Intensity, (b) lifetime, and (c) intensity-weighted lifetime images of two types of green fluorescent beads. (d) Example decays and monoexponential fits to the areas indicated in (b), yielding average lifetimes of 2.21±0.04 and 3.54±0.14 ns for the two types of beads. (e) A histogram of lifetimes in the whole stack shows peaks at 2.23 ns and 3.56 ns. In (a,c) gamma has been adjusted for better visualisation of dimmer beads. (f) Intensity-weighted FLIM volume image, obtained by volume sweep imaging, of fluorescent beads and quantum dots, showing lifetime contrast between fluorescent beads (blue/green) that have shorter fluorescence lifetime, and quantum dots (yellow/red) with longer fluorescence lifetime. (g-i) Cross-sections of the stack in (f).

3.3 | Cancer cell spheroids

3.3.1 | Slice-by-slice imaging

Fig 4 shows TCSPC FLIM images of cancer cell spheroids acquired with the delay line anode detector. The MCF-7 cells were expressing GFP-lifeact, labelling the spheroids throughout with GFP, while the outer surface of the spheroids was labelled with Alexa-488. A total of 31 slices were acquired at 10 μm intervals through the spheroid with data acquisition time 2 minutes per slice. Images of spheroids with both of these labels show nearly uniform intensity where the labels cannot be separated by intensity (Fig 4 a), but the distribution of the two labels can be seen as a gradient in the lifetime (Fig 4 b,c) with the shorter GFP lifetime contributing mostly in the middle of the spheroid and the longer Alexa-488 lifetime contribution increasing towards the edges. Control experiments were performed with spheroids that had the GFP (Fig 4 d) or Alexa-488 (Fig 4 e) label only.

The fluorescence decays, averaged over the images Fig 4 c-e, are shown in Fig 4 f. The average fluorescence lifetimes obtained from biexponential fits to these decays are $\bar{\tau}_{\mathrm{GFP}}$=2.39 ns and $\bar{\tau}_{\mathrm{A488}}$=3.41 ns for the GFP and Alexa-488 in the control

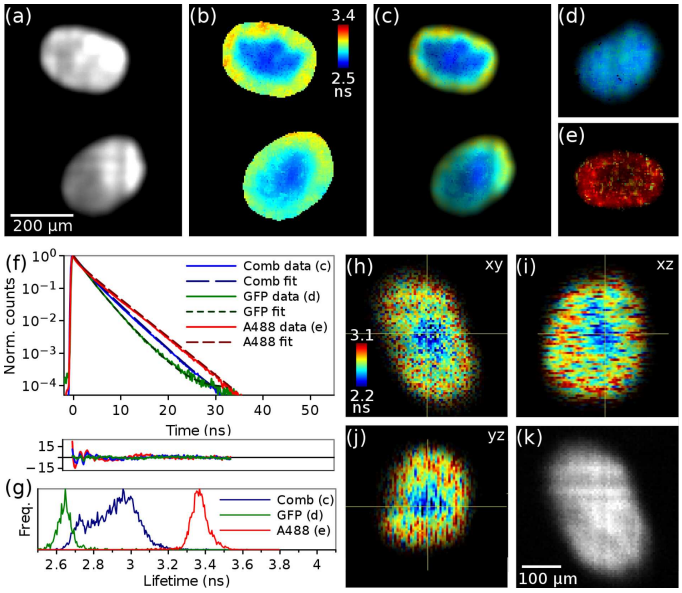

FIGURE 4 Lightsheet FLIM images of cancer cell spheroids, where the cells were labelled with GFP-lifeact (shorter lifetime), and the outer surface of the spheroid with Alexa-488 (longer lifetime). (a) Intensity, (b) lifetime and (c) intensity-weighted lifetime images the spheroids with both labels, and (d-e) images of control spheroids with only (d) GFP or (e) Alexa-488. (f) Fluorescence decays, biexponential fits to the data and residuals of the fits for images (c-e), and (g) histograms of the lifetime values in images (c-e). In (f,g) the data has been averaged over the whole image. (h-k) Volume sweep FLIM images of the spheroids with both GFP and Alexa-488 labels: (h-j) orthogonal views through the lifetime stack, and (h) intensity image of the same xy slice.

samples with single label (Fig 4 d,e), while the average lifetime for the sample with both labels is 2.88 ns. In the lifetime histogram (Fig 4 g) the lifetimes from the GFP and Alexa-488 control images are well separated with narrow peaks at 2.65 ns and 3.36 ns, respectively. The histogram for the image with both fluorophores is broad, as expected, and shows a minor peak at 2.7 ns corresponding to the spheroid centre with mostly GFP contributing, and then a steady increase towards an average lifetime of 3 ns corresponding to the Alexa-488 label gradient towards the surface. See Supplementary Information for the whole stack.

3.3.2 | Volume sweep imaging

The spheroids were also imaged in the volume sweep mode. The 300 μm deep volume was imaged in 5 minutes, and divided into 65 slices with 4.6 μm spacing and data acquisition time of 5 s/slice. A total of 6.56 million photons were collected, corresponding to count rate of 21.5 kHz. Fig 4 h-k shows a slice from this stack, where the intensity image (k) looks uniformly bright but the lifetime image (h-j) shows the lifetime gradient from the shorter GFP lifetime only in the middle to higher lifetime with increasing Alexa-488 contribution towards the spheroid surface. Although the method of moments is not as precise as the exponential fitting method and does not allow multicomponent lifetime analysis, the gradient in the lifetime is clearly visible. See Supplementary Information for the whole stack.

3.4 | *C. elegans*

Fig 5 shows TCSPC FLIM images of living *C. elegans* expressing GFP and stained with Acridine Orange (AO). A stack was acquired with the delay line anode detector with 25 μm spacing and 2 minutes acquisition time per slice. The count rates were comparable to the other experiments; for example, a total of 4.5 million photon were collected with count rate of 37.8 kHz for the slice in Fig 5 a. Lifetimes were obtained by fitting a double exponential function to each pixel of the image.

C. elegans expressing GFP and stained with AO (Fig 5 a,b,e) have an inhomogeneous distribution of lifetimes throughout the length of the worm with an average lifetime of 4.19 ns. The *C. elegans* containing only AO (Fig 5 c) or GFP (Fig 5 d) have higher and lower lifetimes of 4.47 ns and 4.03 ns, respectively. See Supplementary Information for example stacks.

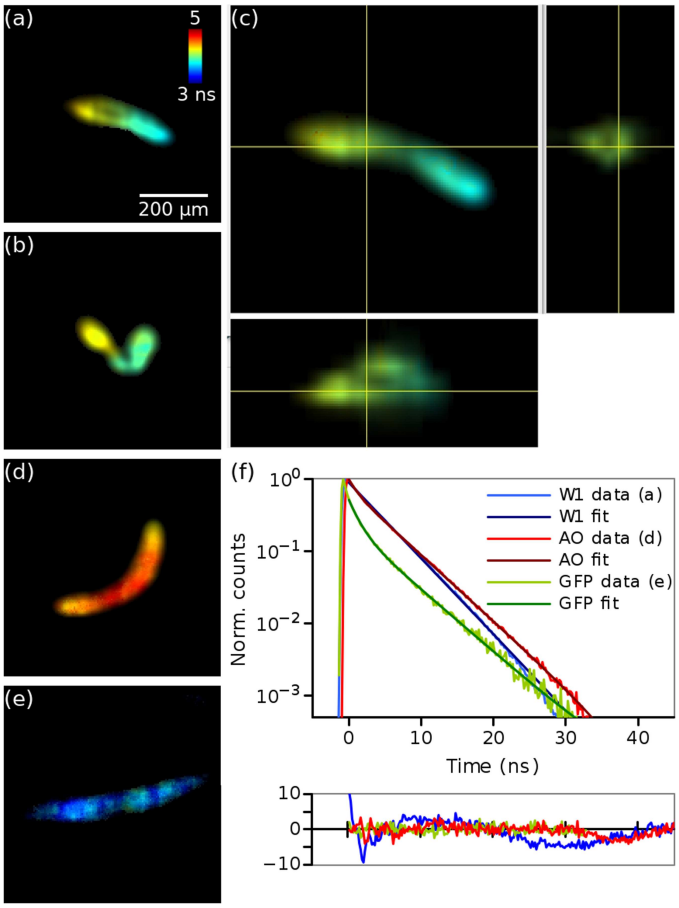

FIGURE 5 Lightsheet FLIM images of *C. elegans*. Slices from 10 a stack (a,b) and orthogonal views (e) of a stack of *C. elegans* expressing GFP and stained with AO, and images of worms stained only with AO (c) or only expressing GFP (d). (f) Time decays, biexponential fits to the data and residuals of the fits for images (a=W1,c=AO,d=GFP). Spatial scale in images (b-d) and lifetime scale in all images is the same as in (a).

4 | DISCUSSION

We have combined lightsheet microscopy with a TCSPC-based wide-field FLIM detector, and illustrated its applications by imaging cancer cell spheroids and *C. elegans*. Lightsheet microscopy enables optical sectioning of thick biological samples embedded in 3D environment while reducing photobleaching of the sample by illuminating only the imaged plane, whereas FLIM provides contrast based on the microenvironment of the probe or proximity of other fluorophores (i.e. FRET). As the low excitation volume and low excitation power yield a limited photon count rate, a photon counting approach is indispensable.

Biochemical tools to study protein interactions do not provide spatial or temporal information. Whilst protein interactions can be studied with biochemical assays, they compromise the cell, and, unlike imaging, do not provide dynamic information in real time about protein or cell stimulation upon addition of extracellular factors. Biochemistry is also not possible in some conditions, e.g. where two different cell types are cultured together.

In this work, the microscope optics were designed to allow a large field of view of ∼1.5 mm diameter to be imaged, with 4 μm pixel size in the sample plane. The pixel size and magnification can be changed according to the sample requirements, for example higher magnification could be used if single cell resolution is required. The image quality and resolution could also be improved by adopting different lightsheet illumination methods, for example illuminating the sample from both sides.

We have applied two different methods for lifetime calculation. The conventional fitting methods provide high accuracy and precision that are needed for complex multicomponent lifetime analysis. Picosecond photon timing capabilities of the MCP combined with fast timing electronics allow IRF widths of a few hundred picoseconds to be achieved, ideal for nanosecond fluorescence lifetime measurements. The volume sweep imaging mode, on the other hand, where the lifetime is obtained with

the method of moments, allows the acquisition of whole FLIM stacks of large 3D volumes in time scale of a few minutes – ideal for real-time monitoring of living specimen.

Furthermore, it is possible to improve the overall data acquisition time. In our 40 mm diameter detector the length of the delay line restricts the data collection window to 100 ns, therefore the detector was operated at an excitation repetition rate of 10 MHz. Only one photon per excitation period can be timed, and to avoid photon pile-up we have chosen to limit the count rate to <1% of the excitation repetition rate, therefore the count rate in these experiments was limited to 10^5 Hz. It is possible to decrease the size of the detector area from 40 mm to 25 mm and operate this delay line in faster mode at 50 MHz repetition rate,[29] yielding maximum count rate of 5×10^5 Hz, and shortening the fast mode stack acquisition time from the 5 minutes demonstrated here to just 1 minute. This could be further improved by pile-up inspection[43] or advanced read-out architectures.[44]

A distinctive advantage of wide-field TCSPC is extremely low, uniformly distributed illumination intensity. In these experiments, 0.1-1 μW excitation power, adjusted according to the sample brightness, was distributed uniformly over the field of view, yielding a maximum intensity of ~0.5-5 mW/cm^2. This is significantly lower than 200 mW/cm^2 reported for gate scanning lightsheet FLIM[10] or the sun's irradiance of the earth, 100 mW/cm^2.

The applications shown in this manuscript could easily be expanded. Spheroids are often used in cancer studies as a model of real tumour. Here the spheroids were fixed to allow immunolabelling of the spheroid surface, but FLIM can be used in living spheroids for monitoring cell cycle,[45] or physiological parameters such as temperature[46] or oxygen concentration.[47] We also demonstrated imaging live *C. elegans* with two fluorescent labels; similar technique could be applied for imaging zebrafish, for example. The low excitation power would also allow continuous long-term imaging.[26,27,48] Moreover, polarized detection of the fluorescence could also be included,[49,50] to perform time-resolved fluorescence anisotropy imaging to map viscosity, or binding and cleavage, via the rotational correlation time, or protein interaction or conformational change via homo-FRET in 3D.

5 | CONCLUSION

We have combined picosecond wide-field TCSPC FLIM with lightsheet microscopy. The microwatt illumination intensity required for TCSPC is significantly lower than other wide-field FLIM methods, and this technique would be ideal for lightsheet microscopy of living organelles, and, for example, measurement of FRET. Besides lightsheet microscopy, this approach is well suited for other specialised illumination microscopy techniques typically employing cameras, such as total internal reflection[30] or supercritical angle fluorescence microscopy.[51] It would also enable FLIM for camera-based super-resolution fluorescence microscopy techniques relying on single fluorophore localisation, and combine single-particle tracking measurements with lifetime measurements.

ACKNOWLEDGMENTS

The authors thank Simon Ameer-Beg (King's College London, UK) for the fluorescent beads, and Roland Wedlich-Soldner (Max Planck Institute of Biochemistry, Martinsried, Germany) for the GFP-lifeact construct. LMH and KS gratefully acknowledge funding from EPSRC Impact Acceleration Account scheme and KS and JN acknowledge BBSRC funding (BB/R004803/1). LMH and SC acknowledge funding from Human Frontier Science Program (grant number RGP0035/2016).

Financial disclosure

None reported.

Conflict of interest

The authors declare no potential conflict of interests.

SUPPORTING INFORMATION

The following supporting information is available as part of the online article:

beads1-slowStack.avi Stack of 2 types of green fluorescent beads acquired slice by slice, 44 slices at 10 μm intervals with data acquisition time 2 minutes per slice. Lifetime scale 1.7-4.2 ns, left=intensity, right=lifetime.
spheroid1-slowStack.avi Stack of a cancer cell spheroid acquired slice by slice, 31 slices at 10 μm intervals with data acquisition time 2 minutes per slice. Lifetime scale 2.5-3.4 ns.
spheroid2-fastStack.avi Fast FLIM stack of a cancer cell spheroid, left=intensity, right=lifetime. 65 slices at 4.6 μm intervals with data acquisition time 5 seconds per slice. Lifetime scale 2.2-3.1 ns.
worm-XX.avi Stacks of *C. elegans* acquired slice by slice. "AO" and "GFP" are controls with one label only, "resXX" have both labels. Lifetime scale 3-5 ns.

References

[1] A. Le Marois, K. Suhling, *Quantitative Live Cell FLIM Imaging in Three Dimensions in "Multi-Parametric Live Cell Microscopy of 3D Tissue Models"*, Springer Berlin Heidelberg, **2017**.

[2] G. McConnell, J. Trägårdh, R. Amor, J. Dempster, E. Reid, W.B. Amos, *eLIFE* **2016**, *5:e18659*.

[3] G. McConnell, W.B. Amos, *J Microsc* **2018**, *270* (2), 252 – 258.

[4] *See http://www.nature.com/nmeth/collections/lightsheetmicroscopy/index.html for a collection of articles.*

[5] R. A. Zsigmondy, *Nobel Lectures, Chemistry 1922-1941*, Elsevier Publishing Company, Amsterdam, **1966**, chapter Properties of Colloids.

[6] Y. S. Hu, M. Zimmerley, Y. Li, R. Watters, H. Cang, *ChemPhysChem* **2014**, *15* (4), 577–586.

[7] J. Huisken, D. Y. R. Stainier, *Development* **2009**, *136* (12), 1963–1975.

[8] K. Greger, M. J. Neetz, E. G. Reynaud, E. H. Stelzer, *Opt Express* **2011**, *19* (21), 20743–20750.

[9] C. A. Mitchell, S. P. Poland, J. Seyforth, J. Nedbal, T. Gelot, T. Huq, G. Holst, R. D. Knight, S. M. Ameer-Beg, *Opt Lett* **2017**, *42* (7), 1269–1272.

[10] P. Weber, S. Schickinger, M. Wagner, B. Angres, T. Bruns, H. Schneckenburger, *Int J Mol Sci* **2015**, *16* (3), 5375–5385.

[11] T. Funane, S. S. Hou, K. M. Zoltowska, S. J. van Veluw, O. Berezovska, A. T. N. Kumar, B. J. Bacskai, *Rev Sci Instrum* **2018**, *89* (5), 053705.

[12] E. Gratton, S. Breusegem, J. Sutin, Q. Ruan, N. Barry, *J Biomed Opt* **2003**, *8* (3), 381–390.

[13] J. Philip, K. Carlsson, *J Opt Soc Am A* **2003**, *20* (2), 368–379.

[14] A. Esposito, H. C. Gerritsen, F. S. Wouters, *J Opt Soc Am A* **2007**, *24* (10), 3261–3273.

[15] H. C. Gerritsen, N. A. H. Asselbergs, A. V. Agronskaia, W. G. J. H. M. Van Sark, *J Microsc* **2002**, *206* (3), 218–224.

[16] P. M. Birch, L. Moore, X. Li, R. Phillips, R. Young, C. Chatwin, *SPIE Proc* **2016**, 98871O.

[17] J. S. Lapington, *Nucl Instrum Meth A* **2012**, *695*, 410–414.

[18] W. Becker, *Advanced Time-Correlated Single Photon Counting Techniques*, Springer Berlin Heidelberg, **2005**.

[19] D. V. O'Connor, D. Phillips, *Time-correlated single-photon counting*, Academic Press, New York, **1984**.

[20] L. M. Hirvonen, K. Suhling, *Meas Sci Technol* **2017**, *28* (1), 012003.

[21] A. S. Tremsin, J. V. Vallerga, O. H. W. Siegmund, *Nucl Instrum Meth A* **2020**, *949*, 162768.

[22] J. S. Lapington, *Nucl Instrum Meth A* **2004**, *525* (1-2), 361–365.

[23] X. Michalet, R. A. Colyer, G. Scalia, A. Ingargiola, R. Lin, J. E. Millaud, S. Weiss, O. H. Siegmund, A. S. Tremsin, J. V. Vallerga, A. Cheng, M. Levi, D. Aharoni, K. Arisaka, F. Villa, F. Guerrieri, F. Panzeri, I. Rech, A. Gulinatti, F. Zappa, M. Ghioni, S. Cova, *Philos T R Soc B* **2013**, *368* (1611), 20120035.

[24] J. Vallerga, J. McPhate, A. Tremsin, O. Siegmund, *Astrophys Space Sci* **2009**, *320* (1-3), 247–250.

[25] S. Stepanov, S. Bakhlanov, E. Drobchenko, H-J. Eckert, K. Kemnitz, in *Laser Applications in Life Sciences*, (Eds: Matti Kinnunen, Risto Myllylä), International Society for Optics and Photonics, SPIE, **2010**, pp. 261–280.

[26] R. Hartig, Y. Prokazov, E. Turbin, W. Zuschratter, *Methods Mol Biol* **2014**, *1076*, 457–480.

[27] M. Vitali, F. Picazo, Y. Prokazov, A. Duci, E. Turbin, C. Götze, J. Llopis, R. Hartig, A. J. Visser, W. Zuschratter, *PLoS ONE* **2011**, *6* (2), e15820.

[28] Z. Petrášek, H.-J. Eckert, K. Kemnitz, *Photosyn Res* **2009**, *102* (2-3), 157–168.

[29] W. Becker, L. M. Hirvonen, J. S. Milnes, T. Conneely, O. Jagutzki, H. Netz, S. Smietana, K. Suhling, *Rev Sci Instrum* **2016**, *87*, 093710.

[30] L. M. Hirvonen, W. Becker, J. Milnes, T. Conneely, S. Smietana, A. Le Marois, O. Jagutzki, K. Suhling, *Appl Phys Lett* **2016**, *109*, 071101.

[31] P. G. Pitrone, J. Schindelin, L. Stuyvenberg, S. Preibisch, M. Weber, K. W. Eliceiri, J. Huisken, P. Tomancak, *Nat Methods* **2013**, *10* (7), 598–599.

[32] J. Milnes, J. S. Lapington, O. Jagutzki, J. Howorth, *Nucl Instrum Meth A* **2009**, *604* (1-2), 218–220.

[33] O. Jagutzki, J. S. Lapington, L. B. C. Worth, U. Spillman, V. Mergel, H. Schmidt-Böcking, *Nucl Instrum Meth A* **2002**, *477* (1-3), 256–261.

[34] P. R. Barber, S. M. Ameer-Beg, J. Gilbey, L. M. Carlin, M. Keppler, T. C. Ng, B. Vojnovic, *J R Soc Interface* **2009**, *6* (Suppl 1), S93–S105.

[35] P. Barber, *SLIM Curve*, http://slim-curve.github.io/.

[36] A. Sillen, Y. Engelborghs, *Photochem Photobiol* **1998**, *67* (5), 475–486.

[37] I. Isenberg, R. D. Dyson, *Biophys J* **1969**, *9* (11), 1337–1350.

[38] L. Xu, Z.-C. Wei, S. Zeng, Z.-L. Huang, *J Innov Opt Health Sci* **2013**, *06* (04), 1350030.

[39] J. Riedl, A. H. Crevenna, K. Kessenbrock, J. H. Yu, D. Neukirchen, M. Bista, F. Bradke, D. Jenne, T. A. Holak, Z. Werb, M. Sixt, R. Wedlich-Soldner, *Nat Methods* **2008**, *5* (7), 605–607.

[40] J. M. Kelm, N. E. Timmins, C. J. Brown, M. Fussenegger, L. K. Nielsen, *Biotechnol Bioeng* **2003**, *83* (2), 173–180.

[41] S. Brenner, *Genetics* **1974**, *77* (1), 71–94.

[42] T. Stiernagle, *C. elegans: A Practical Approach*, Oxford University Press, **1999**, chapter Maintenance of *C. elegans*, pp. 51–67.

[43] C. C. Davis, T. A. King, *J Phys A: Gen Phys* **1970**, *3* (1), 101–109.

[44] O. Jagutzki, A. Cerezo, A. Czasch, R. Dorner, M. Hattass, M. Huang, V. Mergel, U. Spillmann, K. Ullmann-Pfleger, T. Weber, H. Schmidt-Böcking, G. Smith, *IEEE Nucl Sci Conf R* **2001**, *2*, 850–854.

[45] I. A. Okkelman, R. I. Dmitriev, T. Foley, D. B. Papkovsky, *PLOS ONE* **2016**, *11* (12), 1–18.

[46] J. Jenkins, S. M. Borisov, D. B. Papkovsky, R. I. Dmitriev, *Anal Chem* **2016**, *88* (21), 10566–10572.

[47] R. I. Dmitriev, D. B. Papkovsky, *Cell Mol Life Sci* **2012**, *69* (12), 2025–2039.

[48] X. Michalet, R. A. Colyer, J. Antelman, O. H. Siegmund, A. Tremsin, J. V. Vallerga, S. Weiss, *Curr Pharm Biotechnol* **2009**, *10* (5), 543–558.

[49] P. N. Hedde, S. Ranjit, E. Gratton, *Opt Express* **2015**, *23* (17), 22308–22317.

[50] P. N. Hedde, E. Gratton, *Microsc Res Tech* **2018**, *81* (9), 924–928.

[51] T. Barroca, K. Balaa, J. Delahaye, S. Leveque-Fort, E. Fort, *Opt Lett* **2011**, *36* (16), 3051–3053.